How to cite: *Angew. Chem. Int. Ed.* **2022**, *61*, e202113498
International Edition: doi.org/10.1002/anie.202113498
German Edition: doi.org/10.1002/ange.202113498

Electrocatalysis

Nanoconfinement Engineering over Hollow Multi-Shell Structured Copper towards Efficient Electrocatalytical C–C coupling

Chunxiao Liu[+], Menglu Zhang[+], Jiawei Li[+], Weiqing Xue, Tingting Zheng, Chuan Xia,* and Jie Zeng**

Abstract: *Nanoconfinement provides a promising solution to promote electrocatalytic C–C coupling, by dramatically altering the diffusion kinetics to ensure a high local concentration of C_1 intermediates for carbon dimerization. Herein, under the guidance of finite-element method simulations results, a series of Cu_2O hollow multi-shell structures (HoMSs) with tunable shell numbers were synthesized via Ostwald ripening. When applied in CO_2 electroreduction (CO_2RR), the in situ formed Cu HoMSs showed a positive correlation between shell numbers and selectivity for C_{2+} products, reaching a maximum C_{2+} Faradaic efficiency of 77.0 ± 0.3 % at a conversion rate of 513.7 ± 0.7 mA cm^{-2} in a neutral electrolyte. Mechanistic studies clarified the confinement effect of HoMSs that superposition of Cu shells leads to a higher coverage of localized CO adsorbate inside the cavity for enhanced dimerization. This work provides valuable insights for the delicate design of efficient C–C coupling catalysts.*

The anthropogenic fossil fuel consumption and excessive emission of CO_2 have aroused concerns associated with the energy crisis and environmental damage. Direct conversion of CO_2 into value-added chemicals and fuels, powered by renewable electricity, offers a possibility to simultaneously reduce overdependence on fossil fuels and close the anthropogenic carbon cycle.[1–4] Over the past years, major advances have been made in electrocatalytic CO_2 reduction (CO_2RR) to carbon monoxide (CO)[5–8] and formic acid (HCOOH)[9–12] with high yield and near unity selectivity. Compared to C_1 products, deeply reduced C_{2+} products possess higher energy density and market value, thus sparking significant research interest. Copper is recognized as the unique metal to efficaciously break the stable CO_2 bonds and to form C–C bonds, a key step towards C_{2+} products.[13–17] However, due to the sluggish kinetics of multiproton coupled electron transfer and C–C coupling steps, selective conversion of CO_2 into higher-value C_{2+} hydrocarbons and oxygenates at commercially relevant current density (>500 mA cm^{-2}) is still knotty.

The C–C coupling step is greatly affected by the adsorbed CO intermediates (*CO).[18] In general, when a CO_2 molecule is converted to COOH*, the as-derived CO* will dictate the pathway to branch either to C_1 (e.g., CH_4) or C_2 (e.g., C_2H_4, C_2H_5OH) products. Hydrogenation of *CO to *CHO leads to C_1 products, whereas *CO dimerization to form *OCCO embarks on the C_2 pathway.[18] Given that the surface coverage of *CO correlates closely with the dimerization process, one would intend to increase the local concentration of CO to ensure a sufficient coverage of *CO for dimerization. For example, tandem catalysts have been adopted, in which one site produces a high concentration of CO and this is subsequently dimerized to C_2 species on another site.[19,20] An alternative approach is to create a nanoconfinement space in Cu, whereby the intimate contacts and interactions between CO adsorbates increase the incidence of dimerization compared to the open surface.[21,22] Of note, the construction of nanoconfinement depends strongly on morphological control and nanoscale adjustment. Nevertheless, the reported Cu cavities mostly comprise a single layer with large opening holes, leaving a lot of room and chance for the escape of CO adsorbates.[21,22] Moreover, the presence of Cu^+ within the cavity, which is proposed to stabilize CO* and promote dimerization, might complicate the net contribution from nanoconfinement.[22]

Here, we introduce Cu hollow multi-shell structures (HoMSs), with a shell number facilely tunable from 1 to 3, which serve as a simple and flexible platform to decipher the nanoconfinement effects on CO_2RR. Cu HoMSs is an integration of nanoshells layer by layer, with nanovoids confined in between. As the shell number increases, the outflux of carbon species encounters higher diffusion resistance and undergoes longer diffusion path length, rendering the localized C_1 intermediates more vulnerable to dimerization.[23] Enlightened by that, we firstly exerted finite-element method simulations to study the nanoconfinement effect on the distribution of key species of CO_2RR over HoMSs. Experimentally, Cu_2O HoMSs with tunable

[*] C. Liu,[+] M. Zhang,[+] J. Li,[+] W. Xue, T. Zheng, Prof. J. Zeng
Hefei National Laboratory for Physical Sciences at the Microscale, Key Laboratory of Strongly-Coupled Quantum Matter Physics of Chinese Academy of Sciences, National Synchrotron Radiation Laboratory, Key Laboratory of Surface and Interface Chemistry and Energy Catalysis of Anhui Higher Education Institutes, Department of Chemical Physics, University of Science and Technology of China, Hefei, Anhui 230026 (P. R. China)
E-mail: ttzheng@ustc.edu.cn
zengj@ustc.edu.cn
Prof. C. Xia
Yangtze Delta Region Institute (Huzhou), University of Electronic Science and Technology of China, Huzhou 313001 (P. R. China)
E-mail: chuan.xia@uestc.edu.cn
T. Zheng, Prof. C. Xia
School of Materials and Energy, University of Electronic Science and Technology of China, Chengdu 611731 (P. R. China)
[+] These authors contributed equally to this work.

shell numbers were prepared via Ostwald ripening, which were then subjected to in situ reduction under CO_2RR. The as-formed Cu HoMSs showed improved selectivity towards C_{2+} products as the shell number increases, achieving a maximum C_{2+} Faradaic efficiency (FE) of 77.0 ± 0.3 % at a partial current density of 513.7 ± 0.7 mA cm^{-2} in a neutral electrolyte. Mechanistic studies unraveled that superposition of Cu shells led to an increased surface coverage of CO adsorbates for more efficient carbon dimerization, agreeing well with the simulation results.

We anticipate that by increasing the shell numbers of HoMSs, the diffusion kinetics might be dramatically retarded and the retention time of C_1 intermediates prolonged, bolstering the odds for further dimerization into C_2 products. To test the hypothesis, we firstly implemented finite-element method (FEM) simulations to track the key species of CO_2RR over HoMSs. Three models of HoMSs with 1–3 shells were established respectively, to simulate the mass transport of C_1 and C_2 species around individual particle. In the simulations, we posited that CO_2 molecules diffuse into the multi-shell nanostructures, undergo adsorption and then evolve into C_1 species. The C_1 species might either desorb from the surface as a C_1 product, or dimerize to form a C_{2+} product.

With the increase of shell number, we found that more C_1 intermediates are concentrated inside the cavity, substantially enhancing the probability of C–C coupling towards C_2 products (Figure S1). Figures 1a–c show the corresponding C_2/C_1 ratios distributed, respectively, across the three HoMSs, which reveals a positive dependence on the shell numbers (Figure 1d). Specifically, the C_2/C_1 ratio of 3-shell is 5.6 and 1.9 times higher than that of 1-shell and 2-shell, respectively. Moreover, when the simulation parameters such as kinetic constants, equilibrium constants and diffusion coefficients are altered, the trend of C_2/C_1 ratio as a function of shell number still holds (Figure S2). Since the same electric potential was applied over the HoMSs with 1–3 shells (Figure S3), suggesting that the catalytic activities were kept constant, the diffusion process as a function of nanoconfinement might account for the disparity of products distribution. Accordingly, we inferred that although HoMSs with 1-shell might locally confine certain amounts of C_1 adsorbates inside the cavity to form C–C bonds, nevertheless, there is still a big chance for the outflux of desorbed C_1 species as final C_1 products. As such, increasing the shell number could increase the diffusion hurdles and extend the diffusion path length, which effectively restricts the outflux of locally produced C_1 species (Figure S4). As a result, the entrapped C_1 intermediates with a high local concentration could dimerize to C_{2+} products against great odds (Figure 1e). Altogether, the simulation results validate the function of nanoconfinement as a feature of HoMSs on promoting carbon dimerization towards C_{2+} products.

Under the guidance of simulation results, Cu_2O multi-shell nanostructures with different numbers of layers were synthesized. In detail, $CuSO_4$ was used as the Cu precursor and dissolved in water at room temperature, which can be reduced to form Cu_2O nanoparticles by adding $N_2H_4{\cdot}H_2O$ as the reducing agent. Cu_2O single-layer nanoshells were then obtained from the first-step Ostwald ripening process. As illustrated in Figure 2a, after the introduction of N_2H_4 into the reacting solution, newly formed Cu_2O nanocrystallites were assembled inside and outside the first nanoshell layer to form a thicker nanoshell. When a second Ostwald

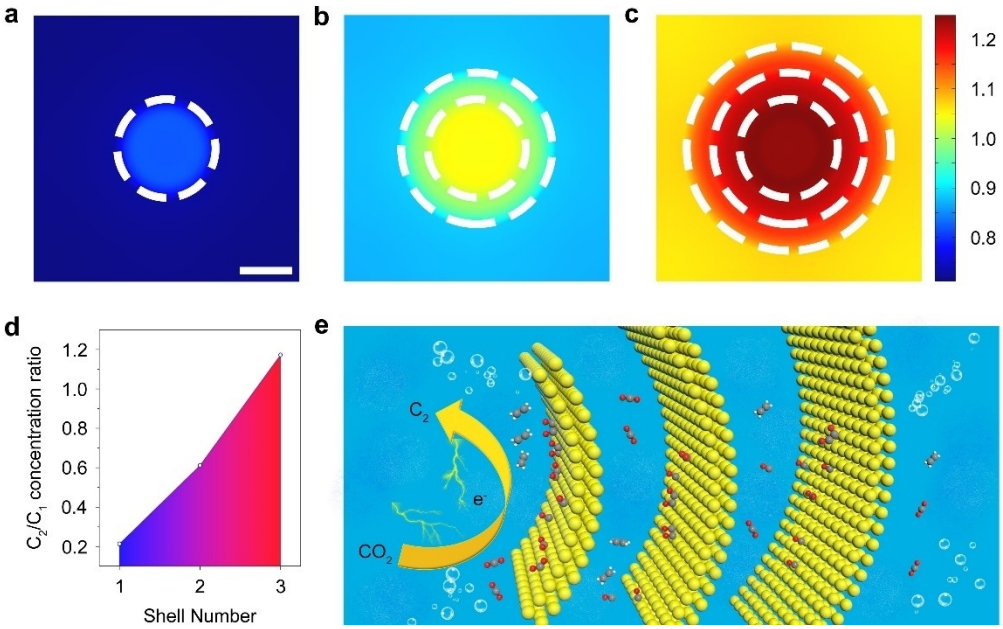

Figure 1. a) The FEM simulated species C_2/C_1 concentration ratio distribution over single 1-shell, b) 2-shell, and c) 3-shell Cu HoMSs, respectively. The white dashed lines represent Cu shells. Scale bar, 100 nm. d) Ratio of C_2/C_1 productivity, measured by the total outflux of C_1 and C_2 products, as a function of shell number. e) Schematic shows how the confinement effect over multi-shell nanostructures promotes C_1 species binding and further conversion to C_2.

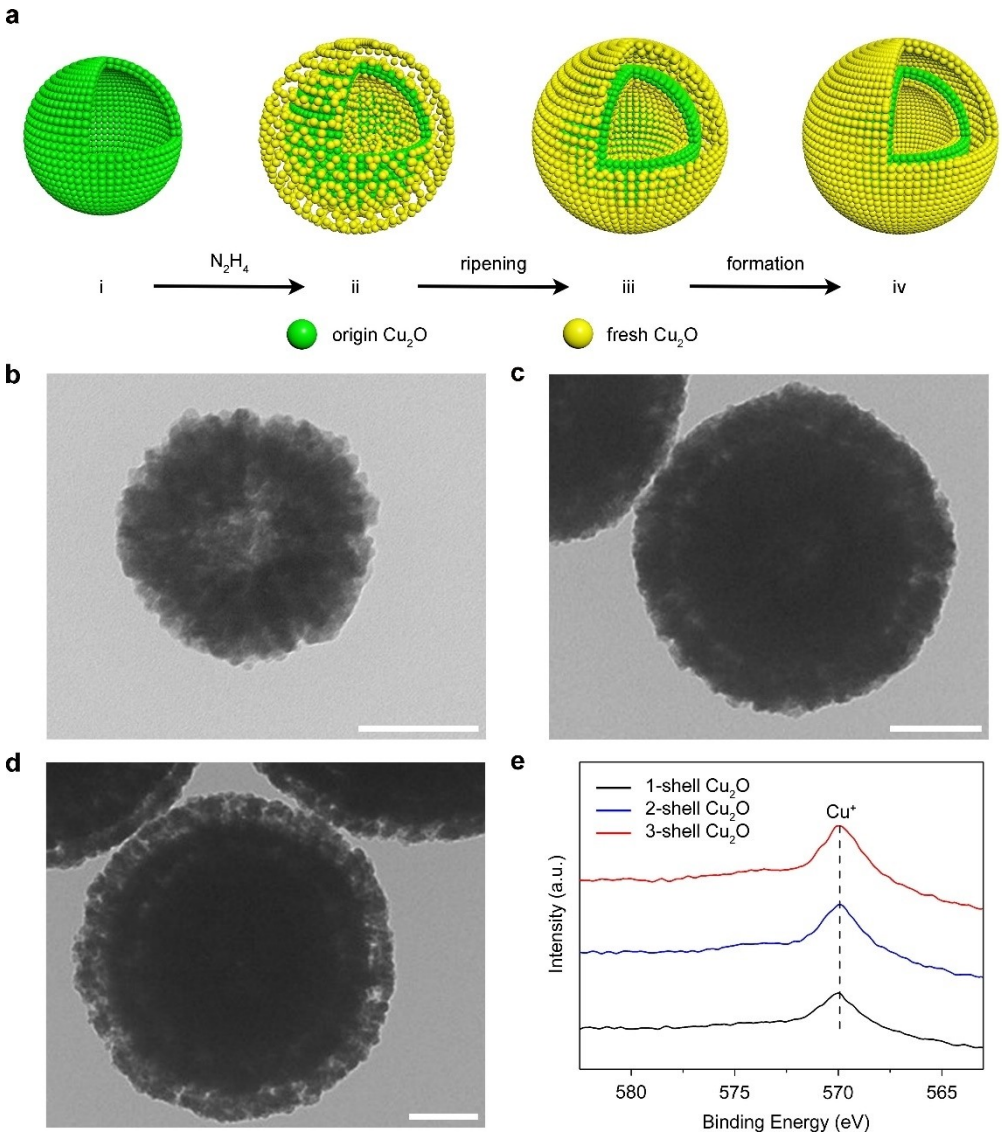

Figure 2. a) Schematic diagram illustrates the design of constructing Cu_2O HoMSs. b) TEM images of 1-shell Cu_2O, c) 2-shell Cu_2O, and d) 3-shell Cu_2O, respectively. Scale bars, 100 nm. e) The X-ray photoelectron spectra of Cu LMM of the as-prepared Cu_2O HoMSs.

ripening process occurred, both the inner and the outer shells would become thinner gradually, leading to the formation of double-shell nanostructures.[24] Nanospheres with rough and porous surface were observed by using scanning electron microscopy (Figure S5). Transmission electron microscope (TEM) images in Figures 2b–d revealed multi-shell nanostructures with single, double and triple layers, respectively. To confirm the chemical state of Cu in the HoMSs, a series of X-ray measurements were conducted on the derived samples. The X-ray diffraction patterns confirmed the cubic Cu_2O phase in all the multi-layer nanoshells (Figure S7). The spectra of Cu 2p (Figure S8) and Auger Cu LMM (Figure 2e) conducted by X-ray photoelectron spectroscopy, taken together, identified the state of Cu^+ in Cu_2O HoMSs.

Catalytic activity and selectivity of HoMSs towards electrocatalytic CO_2 reduction were investigated in a flow reactor using a 0.5 M $KHCO_3$ solution as electrolyte. Before the test, the as-prepared Cu_2O HoMSs loaded on the carbon gas diffusion layers (GDLs) was firstly subjected to an electroreduction under −0.82 V vs. RHE for 10 min, with their morphologies still conserved (Figure S9). Linear scanning voltammetry (LSV) of the as-reduced HoMSs under Ar and CO_2 atmosphere, respectively, were conducted firstly to examine CO_2RR activity by comparing the polarized current, which indicates the kinetics of cathodic reduction. According to the polarization curves measured by LSV, a remarkable enhancement of polarized current in the CO_2 environment was observed (Figure S10). In addition, the reduction current of HoMSs with different layers manifested almost the same intensity, meaning a similar activity to catalyze CO_2RR.

Then the electrolysis gas and liquid products under different potentials were detected by an online gas chroma-

tography and the nuclear magnetic resonance ^{1}H spectrum, respectively. As a result, we obtained an CO_2RR products distribution of HoMSs, involving C_{2+} (C_2H_4, C_2H_5OH, CH_3COOH and C_3H_8O), C_1 (CO and formate) and H_2 (Figure S11). Further analysis delivered the FE and partial current density of C_1 and C_{2+} species over HoMSs towards CO_2RR (Figures 3a,b). The 1-shell HoMSs catalyst exhibited a maximum C_{2+} FE of 40.3 ± 1.0 % at -0.88 V vs. RHE with a C_{2+} current density of 268.8 ± 6.7 mA cm^{-2}. In contrast, the 2-shell HoMSs reached a maximum C_{2+} FE of 62.2 ± 0.3 % with a C_{2+} current density of 414.8 ± 2.2 mA cm^{-2}, while the 3-shell HoMSs sample showed a maximum C_{2+} FE of 77.0 ± 0.3 % with an impressive C_{2+} current density of 513.7 ± 0.7 mA cm^{-2} under the same potential.

As the measured C_{2+}/C_1 ratio summarized in Figure 3c, the increasing shell number clearly promoted the C_{2+} production. In order to exclude the influence of the number of active sites, we compared the intrinsic activities of Cu sites in HoMSs with electrochemical active surface area (ECSA) normalization, which was determined by the underpotential deposition of Pb (Figure S12). The ECSA-normalized C_{2+} partial current density of the three catalysts were also calculated, which substantiated the superior intrinsic activity of 3-shell HoMSs in accordance with our previous conjecture (Figure S13). Moreover, the 3-shell HoMSs catalyst also possessed a conspicuous durability. An 8-hour stability test over 3-shell HoMSs was executed at a constant current density of -300 mA cm^{-2}, where the C_{2+} FE and voltage potentials both remained steady (Figure 3d). The 8-h durability could be attributed to the buffering effect of HoMSs, which enhanced structural tolerance towards disturbance outwards.[23] More remarkably, the morphology of 3-shell HoMSs remained almost intact after long term electrolysis (Figure S14). Considering the unfavorable flooding of carbon GDL, the duration time could be expected to be further extended via loading the catalyst on PTFE membrane.

In an effort to elucidate the real electronic structure of HoMSs under CO_2RR reaction conditions, we conducted in situ X-ray absorption spectroscopy (XAS) measurements. Figure 4a shows the Cu *K*-edge normalized absorption spectra of the HoMSs, which was in situ reduced from Cu_2O HoMSs in a home-made XAS flow cell under -0.82 V vs. RHE (solid lines), or under open circuit potential (dashed lines) for comparison. Copper foil and commercial Cu_2O were adopted as standard samples for Cu^0 and Cu^I reference, respectively. Judging from the shift of adsorption edge and the shape of white line peaks, we inferred that the Cu_2O HoMSs with 1–3 shells were all reduced to metallic Cu from Cu_2O. Furthermore, the extended X-ray absorption fine structure of the HoMSs catalysts indicates that after the negative potential was applied, the peak ascribed to Cu–O bonds disappeared, while the peak representing Cu–Cu bonds appeared (Figure S15). The above results brought forth the conclusion that the active phase of HoMSs under CO_2RR condition is metallic Cu, namely the Cu HoMSs catalyst.

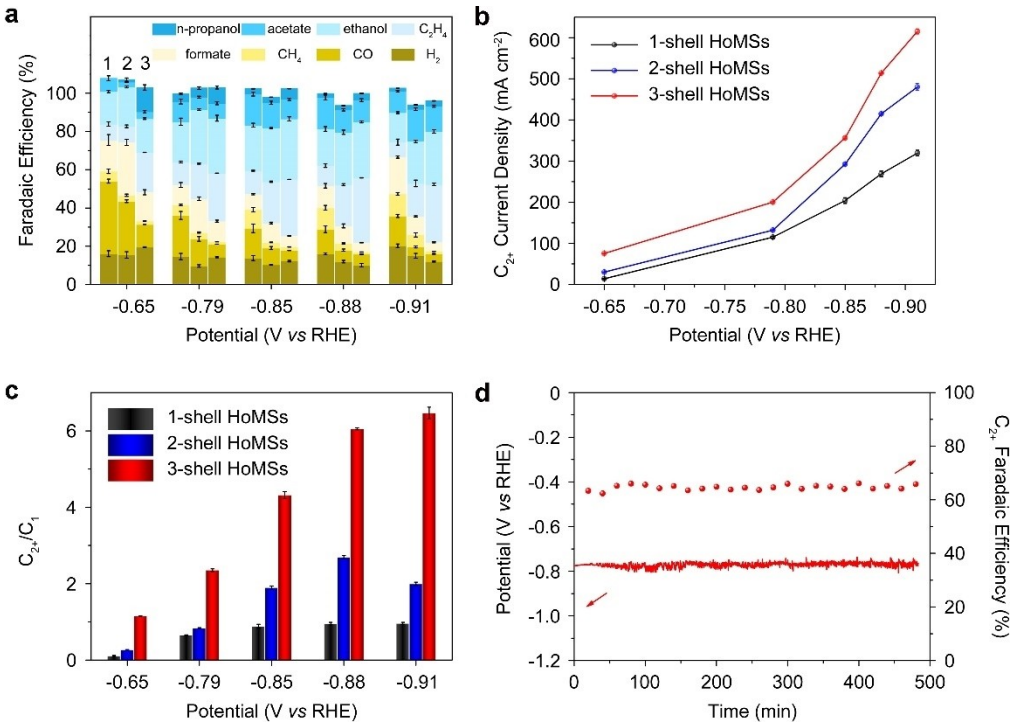

Figure 3. a) CO_2RR products distribution on the catalysts possessing 1–3 shell HoMSs (denoted as 1–3 here, respectively) at different applied potentials. b) C_{2+} partial current densities obtained on HoMSs at different applied potentials. c) C_{2+}/C_1 product selectivity on HoMSs, showing that 3-shell HoMSs has the largest C_{2+} selectivity. d) Durability test of 3-shell HoMSs for 8 h of CO_2-electrolysis in 0.5 M $KHCO_3$ at a current density of -300 mA cm^{-2}.

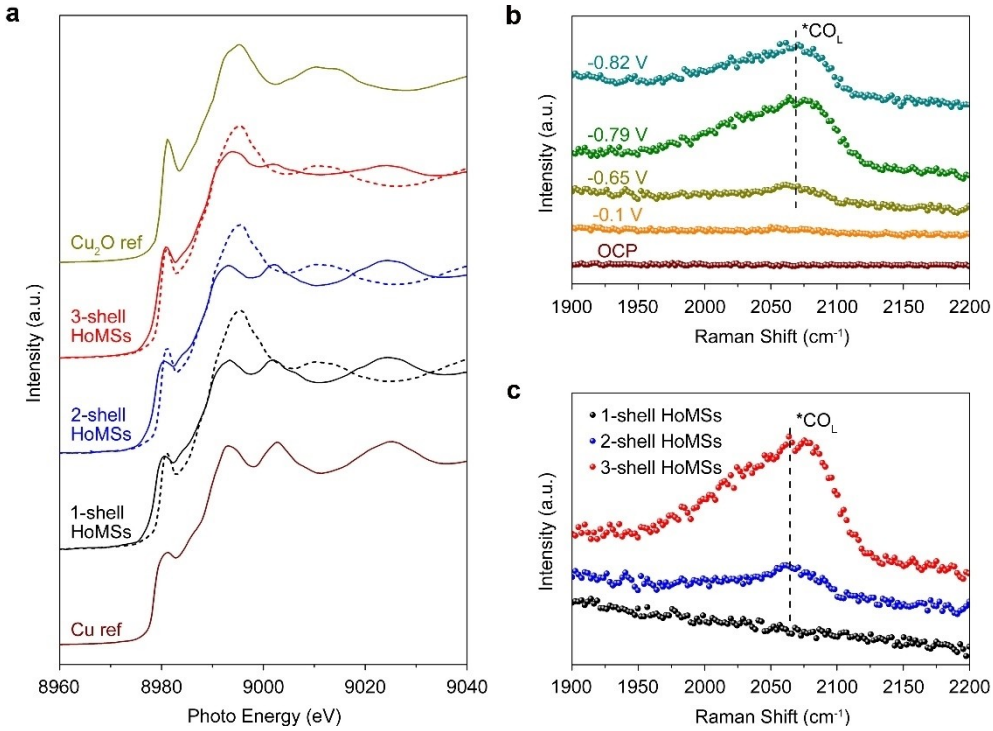

Figure 4. a) In situ Cu K edge X-ray absorption near edge spectra of HoMSs under applied potentials. Ex situ Cu K edge X-ray absorption spectroscopy of Cu_2O and metallic Cu were performed as standards. Among spectra of HoMSs, dashed lines were collected at open circuit potential, while solid lines were collected at −0.82 V vs. RHE. b) In situ Raman spectra of the 3-shell HoMSs catalyst during CO_2RR under different applied potentials. c) Comparison of in situ Raman spectra of 1–3 shell HoMSs at −0.82 V versus RHE in the range of 1900–2200 cm^{-1}.

To shed light on the possible mechanism underlying the confinement effect on CO_2RR, we sought to perform detailed mechanistic studies. At first, a current-step experiment was conducted, where the current was instantly stepped from a reductive current to an oxidative one. The appeared oxidative peak correlates with the oxidation of the localized intermediates.[25] When the intermediates are more locally concentrated, the intensity of the oxidative peak increases accordingly. As the shell number of Cu HoMSs increases, the current step curves under a CO_2 atmosphere show a more intensified oxidative peak (Figure S16). Whereas in the case of 3-shell Cu HoMSs, the oxidative peak was absent under Ar atmosphere. This phenomenon led us to speculate that the Cu HoMSs with more shells are more capable of confining the carbon species.

Then we conducted in situ electrochemical Raman spectroscopy to monitor the surface adsorbates during the CO_2RR process over Cu HoMSs. Figure 4b displays in situ Raman spectra of 3 shell-Cu HoMSs under varied potentials. On scanning the applied potential from −0.1 to −0.82 V vs. RHE over the 3-shell Cu HoMSs catalyst, a notable peak between 2060 cm^{-1} and 2070 cm^{-1} appeared, which was ascribed to the C≡O stretch of the linearly surface-absorbed CO, the key intermediates of C–C coupling.[22] The peak intensities increased on scanning to more negative potentials, in line with the trend of C_{2+} products formation rates (Figure 3b). Moreover, the in situ Raman spectra of the Cu HoMSs with 1–3 shells were compared under the same potential (Figure 4c), where the peak intensity of surface-absorbed CO shows a monotonic increase with the shell number. The observations are consistent with the simulation and CO_2RR results, that superposition of Cu shells led to the increased surface coverage of CO adsorbates for promoting C–C coupling.

The above results, taken together, conclude that the nanoconfinement effect is crucial for the carbon dimerization in CO_2RR. When the reactant species in bulk space influx to the innermost cavity of HoMSs with multi-shells, the confinement space renders the intimate contact and interaction of reactants. Meanwhile, the outflux of as-formed carbon species, restricted by the retarded diffusion kinetics, would suppress desorption of C_1 intermediates, leading to localized C_1 intermediates of high concentration for efficient dimerization towards C_{2+} products. Moreover, considering that the synthesis of HoMSs is flexibly tunable, we anticipate by delicately engineering a cascade catalyst on HoMSs, the C–C coupling could be further dramatically enhanced.[23]

In conclusion, we disclosed a correlation between the CO_2-to-C_{2+} conversion and nanoconfinement effect of Cu HoMSs with the shell number tunable from 1–3. As the shell number increases, the Cu HoMSs displayed a remarkable enhancement in both selectivity and activities towards C_{2+} species. Particularly, Cu HoMSs with 3 shells exhibits a maximum C_{2+} FE of 77.0 ± 0.3 % with an impressive C_{2+} current density of 513.7 ± 0.7 mA cm^{-2} in a neutral electrolyte. Finite-element method simulation combined with experimental mechanistic studies revealed that the increase

of shell number leads to more CO adsorbate trapped inside nanovoids via retarding the diffusion kinetics. The resultant high local concentrations of C_1 intermediates were proposed to facilitate the C–C coupling process. Our work highlights the importance of nanoconfinement in carbon dimerization and provides guidance for designing highly efficient catalysts towards multicarbon products.

Acknowledgements

J.Z. acknowledges National Key Research and Development Program of China (2019YFA0405600), National Science Fund for Distinguished Young Scholars (21925204), NSFC (U19A2015), Fundamental Research Funds for the Central Universities, Provincial Key Research and Development Program of Anhui (202004a05020074), and USTC Research Funds of the Double First-Class Initiative (YD2340002002). C.X. acknowledges the University of Electronic Science and Technology of China (UESTC) for Startup funding (A1098531023601264), and the NSFC (22102018 and 52171201). T.Z. acknowledges NSFC (22005291).

Conflict of Interest

The authors declare no conflict of interest.

Keywords: C–C coupling · CO_2 electroreduction · Diffusion kinetics · Nanoconfinement

[1] S. Chu, Y. Cui, N. Liu, *Nat. Mater.* **2017**, *16*, 16–22.
[2] Y. Y. Birdja, E. Pérez-Gallent, M. C. Figureueiredo, A. J. Göttle, F. Calle-Vallejo, M. T. M. Koper, *Nat. Energy* **2019**, *4*, 732–745.
[3] J. H. Montoya, L. C. Seitz, P. Chakthranont, A. Vojvodic, T. F. Jaramillo, J. K. Nørskov, *Nat. Mater.* **2017**, *16*, 70–81.
[4] H. Shin, K. U. Hansen, F. Jiao, *Nat. Sustainability* **2021**, *4*, 911–919.
[5] J. Gu, C.-S. Hsu, L. Bai, H. M. Chen, X. Hu, *Science* **2019**, *364*, 1091–1094.
[6] T. Zheng, K. Jiang, N. Ta, Y. Hu, J. Zeng, J. Liu, H. Wang, *Joule* **2019**, *3*, 265–278.
[7] X. Wang, Z. Chen, X. Zhao, T. Yao, W. Chen, R. You, C. Zhao, G. Wu, J. Wang, W. Huang, J. Yang, X. Hong, S. Wei, Y. Wu, Y. Li, *Angew. Chem. Int. Ed.* **2018**, *57*, 1944–1948; *Angew. Chem.* **2018**, *130*, 1962–1966.
[8] W. Ren, X. Tan, J. Qu, S. Li, J. Li, X. Liu, S. P. Ringer, J. M. Cairney, K. Wang, S. C. Smith, C. Zhao, *Nat. Commun.* **2021**, *12*, 1449.
[9] L. Li, A. Ozden, S. Guo, F. P. García de Arquer, C. Wang, M. Zhang, J. Zhang, H. Jiang, W. Wang, H. Dong, D. Sinton, E. H. Sargent, M. Zhong, *Nat. Commun.* **2021**, *12*, 5223.
[10] C. Xia, P. Zhu, Q. Jiang, Y. Pan, W. Liang, E. Stavitski, H. N. Alshareef, H. Wang, *Nat. Energy* **2019**, *4*, 776–785.
[11] T. Zheng, C. Liu, C. Guo, M. Zhang, X. Li, Q. Jiang, W. Xue, H. Li, A. Li, C.-W. Pao, J. Xiao, C. Xia, J. Zeng, *Nat. Nanotechnol.* **2021**, https://doi.org/10.1038/s41565-021-00974-5.
[12] Q. Gong, P. Ding, M. Xu, X. Zhu, M. Wang, J. Deng, Q. Ma, N. Han, Y. Zhu, J. Lu, Z. Feng, Y. Li, W. Zhou, Y. Li, *Nat. Commun.* **2019**, *10*, 2807.
[13] C. Chen, X. Yan, S. Liu, Y. Wu, Q. Wan, X. Sun, Q. Zhu, H. Liu, J. Ma, L. Zheng, H. Wu, B. Han, *Angew. Chem. Int. Ed.* **2020**, *59*, 16459–16464; *Angew. Chem.* **2020**, *132*, 16601–16606.
[14] K. Jiang, Y. Huang, G. Zeng, F. M. Toma, W. A. Goddard, A. T. Bell, *ACS Energy Lett.* **2020**, *5*, 1206–1214.
[15] X. Wei, Z. Yin, K. Lyu, Z. Li, J. Gong, G. Wang, L. Xiao, J. Lu, L. Zhuang, *ACS Catal.* **2020**, *10*, 4103–4111.
[16] W. Deng, L. Zhang, L. Li, S. Chen, C. Hu, Z.-J. Zhao, T. Wang, J. Gong, *J. Am. Chem. Soc.* **2019**, *141*, 2911–2915.
[17] C. Peng, G. Luo, J. Zhang, M. Chen, Z. Wang, T.-K. Sham, L. Zhang, Y. Li, G. Zheng, *Nat. Commun.* **2021**, *12*, 1580.
[18] D. Gao, R. M. Arán-Ais, H. S. Jeon, B. R. Cuenya, *Nat. Catal.* **2019**, *2*, 198–210.
[19] H. Zhang, X. Chang, J. G. Chen, W. A. Goddard III, B. Xu, M.-J. Cheng, Q. Lu, *Nat. Commun.* **2019**, *10*, 3340.
[20] X. Wang, J. F. de Araújo, W. Ju, A. Bagger, H. Schmies, S. Kühl, J. Rossmeisl, P. Strasser, *Nat. Nanotechnol.* **2019**, *14*, 1063–1070.
[21] T.-T. Zhuang, Y. Pang, Z.-Q. Liang, Z. Wang, Y. Li, C.-S. Tan, J. Li, C. T. Dinh, P. D. Luna, P.-L. Hsieh, T. Burdyny, H.-H. Li, M. Liu, Y. Wang, F. Li, A. Proppe, A. Johnston, D.-H. Nam, Z.-Y. Wu, Y.-R. Zheng, A. H. Ip, H. Tan, L.-J. Chen, S.-H. Yu, S. O. Kelley, D. Sinton, E. H. Sargent, *Nat. Catal.* **2018**, *1*, 946–951.
[22] P.-P. Yang, X.-L. Zhang, F.-Y. Gao, Y.-R. Zheng, Z.-Z. Niu, X. Yu, R. Liu, Z.-Z. Wu, S. Qin, L.-P. Chi, Y. Duan, T. Ma, X.-S. Zheng, J.-F. Zhu, H.-J. Wang, M.-R. Gao, S.-H. Yu, *J. Am. Chem. Soc.* **2020**, *142*, 6400–6408.
[23] J. Y. Wang, J. Wan, N. Yang, Q. Li, D. Wang, *Nat. Chem. Rev.* **2020**, *4*, 159–168.
[24] L. Zhang, H. Wang, *J. Phys. Chem. C* **2011**, *115*, 18479–18485.
[25] R. He, A. Zhang, Y. Ding, T. Kong, Q. Xiao, H. Li, Y. Liu, J. Zeng, *Adv. Mater.* **2018**, *30*, 1705872.

Manuscript received: October 12, 2021
Accepted manuscript online: November 25, 2021
Version of record online: December 2, 2021